Energy-Efficient TDMA-NOMA for RIS-Assisted Ultra-Dense VLC Networks

Asim Ihsan, Muhammad Asif, Wali Ullah Khan, Isaac N. O. Osahon, and Sujan Rajbhandari, *Senior Member, IEEE*

***Abstract*—This paper proposes an energy-efficient optimization technique for downlink indoor visible light communication (VLC) systems using hybrid non-orthogonal multiple access (NOMA) and reconfigurable intelligent surfaces (RIS). The approach considers a hybrid time division multiple access-NOMA (TDMA-NOMA) to provide massive connectivity to multi-clusters. Clusters of users are formed using NOMA while TDMA is used to allocate a specific time slot within a communication frame. The proposed technique optimizes the precoding at the multi-LED transmitter, RIS tuning parameters, and time-slot allocation parameters for each cluster to maximize the system's energy efficiency (EE). The EE optimization problem is solved through the block coordinate descent (BCD) framework, which splits the optimization problem into two blocks. An alternating optimization (AO) framework is used in the first block to optimize the transmit precoding through conic quadratic programming (CQP) and RIS tuning parameters through a semidefinite programming (SDP) technique based on the surrogate optimization method. The second block allocates energy-efficient time-slot for each cluster through linear programming (LP) approach to further improve the EE of the system. The simulation results indicate that the proposed BCD framework achieves fast convergence and excellent performance in terms of the EE of the system while maintaining low computational complexity.**

***Index Terms*—Energy Efficiency, Hybrid TDMA-NOMA Systems, Reconfigurable Intelligent Surfaces, Resource Allocations, Visible Light Communication.**

I. Introduction

Along with other complementary technologies, visible light communications (VLC) is one primary wireless solution to realise the Sixth Generation (6G) networks offering high-date rate, low latency and energy efficiency (EE) [1]. Utilizing visible wavelengths within the range of 375 nm to 780 nm, VLC systems can concurrently offer illumination and communication. Despite the unlicensed nature of the visible light spectrum, which theoretically provides a bandwidth advantage over the highly congested radio frequency (RF) spectrum, practical limitations with optical transceivers constrain the achievable modulation bandwidth to a range typically around hundreds of MHz [2]. Although VLC networks offer several other advantages, such as low-cost transceivers, improved security, and the absence of electromagnetic interference (EMI), there are significant challengs that need to be addressed to realise its integration with future wireless systems. These challenges include the limited bandwidth of off-the-shelf light emitting diodes (LEDs) and receivers, and significant degradation in performance in non-line-of-sight (NLOS) scenarios [3].

The limited bandwidth issue of the LEDs can be tackled efficiently by adopting spectral efficient non-orthogonal multiple access (NOMA) assisted techniques [4]. NOMA leverages the power domain for user multiplexing. At the transmitter, it utilizes superposition coding (SC) to allocate different power levels to users and combine their signals. Subsequently, at the receiver, successive interference cancellation (SIC) is applied. SIC operates by first detecting and eliminating the highest interference signals successively until the desired signal is detected. However, it's worth noting that as the number of users grows, the complexity of SIC increases due to the rising number of interference signals [5]. Therefore, in practice, to overcome the complexities of employing SIC in a dense network, NOMA is integrated with conventional orthogonal multiple access (OMA) techniques such as orthogonal frequency division multiple access (OFDMA)-NOMA [6] and TDMA-NOMA [7], [8]. These hybrid multiple access techniques have huge potential to provide massive connectivity for beyond fifth generation (5G) wireless networks.

On the other hand, the significant signal degradation issues in VLC can be improved by employing reconfigurable intelligent surfaces (RIS) [9]. RIS-assisted VLC can dynamically and autonomously adapt to achieve ubiquitous connectivity despite adverse probabilistic factors of wireless channels. Integrating RIS into indoor VLC systems can enhance resilience against line-of-sight (LOS) blockages, improve the quality of service (QoS) for communication, mitigate interference, increase EE, and improve localization services [10]. In VLC systems, RIS can be deployed at various locations based on the desired functionality. These deployment choices encompass positioning RIS on the transmitter end [9], the receiver end [11], or in the middle of the transmitter and receiver [12].

System-level optimization is crucial for the transformation of VLC into a scalable and networked wireless technology, enhancing its performance, reliability, and efficiency. Optimization addresses challenges such as interference, multipath fading, and lighting constraints, enabling seamless integration with existing networks. It also supports scalability through resource allocation. VLC's commercial viability is enhanced by optimizing spectral efficiency, power consumption, and deployment costs. Overall, system-level optimization maximizes VLC's potential

This work was supported by the Engineering and Physical Sciences Research Council (EPSRC) through the Platform for Driving Ultimate Connectivity (TITAN), EP/X04047X/1 and EP/Y037243/1.

(Corresponding author: Muhammad Asif .)

Asim Ihsan and Isaac N. O. Osahon are with the Department of Engineering, Electrical Engineering Division, University of Cambridge, Cambridge, U.K. (Email: ai422@cam.ac.uk, and ino20@cam.ac.uk).

Sujan Rajbhandari is with Institute of Photonics, University of Strathclyde, Glasgow, Scotland, U.K. (Email: sujan.rajbhandari@strath.ac.uk; sujan@ieee.org).

Muhammad Asif is with the School of Computer Science and Communication Engineering, Jiangsu University, Zhenjiang, China. (Email: masif@ujs.edu.cn).

Wali Ullah Khan is with the Interdisciplinary Centre for Security, Reliability and Trust (SnT), University of Luxembourg, 1855 Luxembourg City, Luxembourg.(Email: waliullah.khan@uni.lu).

and facilitates its integration into various applications [13]. In the existing literature, numerous studies have investigated into various optimization aspects of VLC systems with RIS, encompassing EE, sum-rate optimization, security enhancement, and link reliability. However, there exists a significant research gap in the literature regarding the development of an optimization framework aimed at enhancing EE for hybrid TDMA-NOMA-based RIS-assisted indoor downlink VLC networks.

A. Related Literature

The VLC systems has primarily focused on improving transmission in uncontrollable channel conditions. However, to achieve 6G key performance indicators (KPIs), VLC systems need to move beyond the limitations of current communication architecture and leverage the wireless environment as an adaptable parameter. This can be achieved through optical manipulators that can be categorized based on their input and output characteristics. Optical radiation manipulation involves changing various properties of propagating waves, such as propagation direction, polarization, phase, amplitude, frequency, spatial power distribution, and wavefront shape [10]. One fascinating application of these manipulators in VLC systems is the ability to focus optical power towards target receivers. These manipulators are generally known as RIS. In VLC systems, mirror-based and metasurface-based RIS are common [14]. Mirror-based RIS comprises of numerous small, adjacent mirrors that can be realized using microelectromechanical systems (MEMS) technology [14]. While metasurface-based RIS are scattering-based manipulators that offer a full range of possibilities for manipulating the various properties of light. These materials are composed of periodic subwavelength metallic or dielectric structures, also known as atoms. The behaviour of metasurfaces is controlled by particle plasmon and Mie resonances that are designed to manipulate light by scattering it through these subwavelength elements [10].

Inspired by the positive outcomes of NOMA in RF networks [15], researchers have recognized its potential to enhance the performance of VLC systems by achieving higher spectral and energy efficiency. The superiority of NOMA-enabled VLC systems over OMA-enabled VLC systems in terms of energy efficiency [16], and sum rate [17] gains has been demonstrated. The adoption of NOMA in VLC systems is promising for several reasons. First, the modulation bandwidth of LED (a typical VLC transmitter) is limited, which alters achievable data rates. Second, NOMA's efficiency to efficiently multiplex a small number of users is well-suited for most indoor VLC networks, where each Access Point (AP) typically covers only a few users. Third, VLC systems provide ample opportunities for enhancing the variations in channel gain among users through various techniques, which is vital in NOMA. It offers several ways to optimize the angles of incidence and irradiance through angle diversity transceivers, tuning the Field-of-View (FoV) of the transceivers, to enhance the channel gain variations among users. Fourth, NOMA's accuracy in Channel State Information (CSI) is crucial for superposition coding in NOMA. In VLC systems, securing accurate CSI proves to be advantageous as the channel exhibits a high degree of stability, due to low mobility of users commonly observed in indoor environments. Fifth, NOMA performs better in high Signal-to-Noise Ratio (SNR) scenarios [4], and VLC systems can provide high SNR when LoS paths exist, owing to the short distance between the transmitter and the receiver.

The integration of RIS in NOMA-based VLC systems can enhance performance gains due to the following reasons [14]: (i) It can create distinct channel and improve the channel conditions of users, which is essential for outperforming OMA, resulting in superior performance gains; (ii) RIS can optimize the channel gains of far users, enabling the sorting of users based on their data rate requirements.; (iii) RIS can also extend the coverage area of the VLC AP, enhancing the quality of the channel for users located beyond the illuminated region. To meet the demands of future wireless networks, significant efforts are needed on the system-level optimization of RIS-enabled VLC systems. The work in [18] maximized the energy efficiency of the TDMA-based RIS-enabled VLC system under unique power constraints. The proposed optimization algorithm optimizes time allocation, power control, and phase shift matrix. The sum rate of the OMA-based RIS-aided VLC system is maximized in [19]. An association matrix is introduced to simplify the allocation problem of RIS units to LEDs. The problem is reduced to a binary programming problem, which is solved with a low-complexity algorithm that maximizes the achievable sum rate. For the NOMA-based RIS-enabled VLC network, the sum rate is maximized in [20]. The authors in [21] proposed a joint optimization framework for NOMA and RIS parameters for RIS-enabled NOMA-based VLC system that results in significant improvements in link reliability. The authors in [22] have shown that optimizing both the RIS configuration and NOMA power allocation simultaneously can improve the secrecy capacity of the RIS-enabled NOMA-based system while also reducing the risk of eavesdropping by malicious network users.

Building on the advancements in RIS-enabled NOMA systems, recent research has also explored the integration of RIS in hybrid TDMA-NOMA frameworks. Existing studies on RIS in hybrid TDMA-NOMA systems have made significant contributions, each addressing different aspects of the integration. For instance, [23] and [24] investigated reflective RIS in wireless-powered scenarios, while [26], [27], [30], examined the application of simultaneously transmitting and reflecting (STAR)-RIS in mmWave and cellular networks. Notably, [29] utilized reflective RIS in multi-LED optical systems, focusing on capacity maximization in VLC sytem. In contrast, our work integrates a reflective RIS with multi-LED optical transmission, addressing energy efficiency and incorporating advanced time-allocation and precoding strategy. This approach distinguishes our study by advancing the capabilities of hybrid TDMA-NOMA systems in VLC environments, thereby filling gaps identified in the current literature. A detailed comparison of our proposed scheme with related works is provided in Table I.

B. Motivations and Contributions

The future 6G networks are expected to overcome the limitations of current technologies to fulfil the demand for energy-efficient, high-speed and scalable wireless communications. The hybrid TDMA-NOMA system has recently emerged as a potential solution for enabling massive connectivity and meeting the demanding rate requirements of future 6G networks [7].

TABLE I: Comparison of proposed scheme and related works

	RIS Type	TDMA-NOMA	Transmitter Antennas	Communication Type	VLC	Energy-efficiency	Precoding	time-allocation
[23]	Reflective	✓	Single	Wireless-Powered				
[24]	Reflective	✓	Single	Wireless-Powered				✓
[25]	Reflective	✓	Single	URLLC				
[26]	STAR-RIS	✓	Multi	mmWave			✓	✓
[27]	STAR-RIS	✓	Single	Cellular				✓
[28]	Reflective	✓	Single	Cellular				
[29]	Reflective	✓	Multi-LED	Optical	✓			
This work	Reflective	✓	Multi-LED	Optical	✓	✓	✓	✓

However, despite their potential, challenges such as interference management, energy efficiency, and coverage limitations in NLOS scenarios remain significant barriers. The integration of RIS into hybrid TDMA-NOMA systems offers a novel approach to overcome these limitations by dynamically optimizing the wireless environment and enhancing spectral efficiency [23]–[29]. While existing research has addressed various aspects of RIS-enabled VLC, such as energy efficiency [18], sum rate maximization [19], [20], security enhancement [22] and link reliability [21], there is a gap in the literature when it comes to an energy-efficient resource allocation optimization framework for hybrid TDMA-NOMA-based RIS-assisted multi-LED downlink VLC systems. Although research work in [18] have focused on maximizing the energy efficiency of RIS-enabled VLC systems using the TDMA technique. However, the exploration of the hybrid TDMA-NOMA scheme in this context remains limited in the literature. Therefore, this manuscript proposes a novel energy-efficient BCD framework for EE maximization of hybrid TDMA-NOMA-based RIS-Assisted downlink VLC systems. Our major contribution is summarized as follows,

- A novel energy-efficient BCD optimization framework for the hybrid TDMA-NOMA-based RIS-Assisted downlink VLC system is proposed. The EE of the system is maximized through BCD in two blocks. In first block, alternating optimization (AO) framework is employed which alternatively optimizes the transmit precoding of the multi-LED transmitter through conic quadratic programming (CQP), and RIS tunning parameters through semi definite programming (SDP) that exploits surrogate optimization method. The second block optimizes the time-slot allocations for each cluster through linear programming (LP) approach to further improve the energy efficiency of the system. The optimization of the system is done under the required system constraints. The system constraints include illumination and optical power of LEDs, SIC-decoding, data rate, power budget, TDMA time-slot allocation and RIS tunning parameter.
- The proposed algorithm's worst-case computational complexity is computed in terms of Big O notation which is low-complex for practical implementations.
- The simulation results present that proposed optimization framework yields exceptional EE performance for the RIS-assisted hybrid-NOMA VLC system. Additionally, our proposed framework effectively achieves convergence in only a few iterations while satisfying all the system constraints.
- In contrast to prior research in TDMA-NOMA-based VLC systems, which often assumes equal time-slot allocation across various NOMA users clusters, our research addresses a critical limitation. We introduce a novel algorithm that offers energy-efficient time-slot allocation, considering the diverse channel conditions and QoS constraints of different NOMA user clusters. By doing so, our approach significantly enhances system performance.

II. SYSTEM MODEL

In this section, we consider the system model of RIS-assisted downlink hybrid TDMA-NOMA VLC system as illustrated in Fig. 1. The transmitter consists of evenly-spaced L LED 2-D arrays that transmit its signals to K single-photodiode users. The RIS with N reflecting elements is also deployed to assist the downlink communication. The transmitter and RIS are connected through a controller to coordinate and transmit the information to multiple users simultaneously [31]. The total transmittion time (t_T) of the system is shared by J time-slots, where $\mathcal{T} = \{t_j | j = 1, 2, \ldots, J\}$. According to the NOMA principles, multiple users can be served on the same time-slot. The group of users on t_j is known as cluster. The J time-slots result in I clusters in the system. The number of users served through t_j is K_j, where $\sum_{j=1}^{J} K_j = K$. Moreover, the system model considers the size of the room, which can be expressed as $L \times W \times H$ cubic meters, where L is the length, W is the width, and H is the height. To deploy the LEDs, the ceiling of the room divided into perfect squares, and LEDs were placed in the center of each square. For the RIS, an array of $n \times n$ identical rectangular optical metasurface patches used,which are evenly fixed in a rectangular frame, placed on a vertical surface of one side of the wall. Moreover, the users were randomly deployed in the room, and their locations were modeled as a binomial point process (BPP).

A. CHANNEL MODEL

The channel gain of the system consists of LoS and NLoS paths which are presented in this section. The location of l^{th} LED, k^{th} user, and n^{th} RIS units in a three-dimensional Cartesian coordinate system are $(x^l_{LED}, y^l_{LED}, z^l_{LED})$, $(x^k_{user}, y^k_{user}, z^k_{user})$, and $(x^n_{RIS}, y^n_{RIS}, z^n_{RIS})$, respectively. Then, the distance between l^{th} LED and k^{th} user can be expressed as

$$d_{k,l} = \sqrt{(x^k_{user} - x^l_{LED})^2 + (y^k_{user} - y^l_{LED})^2 + (z^k_{user} - z^l_{LED})^2}, \quad (1)$$

and those of l^{th} LED to n^{th} RIS element and n^{th} RIS element to k^{th} user distance is given by

$$d_{n,l} = \sqrt{(x^n_{RIS} - x^l_{LED})^2 + (y^n_{RIS} - y^l_{LED})^2 + (z^n_{RIS} - z^l_{LED})^2}, \quad (2)$$

$$d_{k,n} = \sqrt{(x^k_{user} - x^n_{RIS})^2 + (y^k_{user} - y^n_{RIS})^2 + (z^k_{user} - z^n_{RIS})^2}. \quad (3)$$

It is assumed that the normal vectors of the transceivers are perpendicular to the ground, and therefore the angle of irradi-

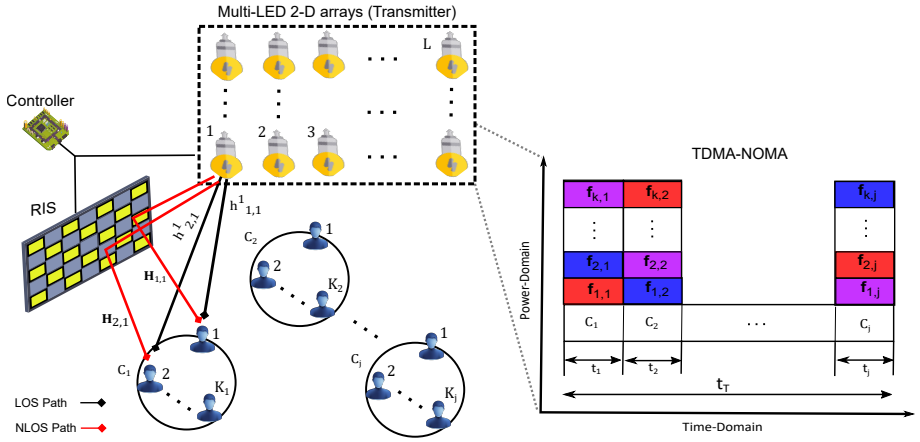

Fig. 1: System model illustrating TDMA-NOMA operation in RIS-assisted ultra-dense VLC networks.

ance $\Theta_{k,l}^{LoS}$ and incidence $\phi_{k,l}^{LoS}$ of each LoS component of the channel gain are expressed as

$$\Theta_{k,l}^{LoS} = \phi_{k,l}^{LoS} = \arccos(\frac{z_{LED}^{l} - z_{user}^{k}}{d_{k,l}}). \tag{4}$$

Similarly, the angle of irradiance of l^{th} LED and n^{th} RIS element NLoS path can be given by

$$\Theta_{n,l}^{NLoS} = \arccos(\frac{z_{LED}^{l} - z_{RIS}^{n}}{d_{n,l}}), \tag{5}$$

and NLoS path angle of incident at the k^{th} user can be written as

$$\phi_{k,n}^{NLoS} = \arccos(\frac{z_{RIS}^{n} - z_{user}^{k}}{d_{k,n}}). \tag{6}$$

Now, the LoS channel gain between l^{th} LED and k^{th} user at SC_j can be modelled through Lambertian radiant formulation as follow [32]:

$$h_{k,l}^{j} = \begin{cases} \frac{(m+1)A_D G_f R_D}{2\pi d_{k,l}^2} \cos^m(\Theta_{k,l}^{LoS}) \cos(\phi_{k,l}^{LoS}) g(\phi_{k,l}^{LoS}), \\ 0 \le \phi_{k,l}^{LoS} \le \phi_{FoV}; \\ 0, \qquad \text{Otherwise.} \end{cases} \tag{7}$$

where m presents Lambertian index which can be determined by half intensity radiation angle of the transmitter $\psi_{1/2}$ as $m = \frac{-1}{\log_2(\cos(\psi_{1/2}))}$. A_D, G_f, and R_D are the physical area of the detector, a gain of the optical filter and the responsivity of the detector, respectively. $d_{k,l}$ denotes the Euclidean distance between the l^{th} LED and the k^{th} user. ϕ_{FoV} represents the field of view (FoV) of the detector. $g(\phi_{k,l})$ is the optical concentrator gain that can be expressed as

$$g(\phi_{k,l}^{LoS}) = \begin{cases} \frac{r^2}{\sin^2(\phi_{FoV})}, & 0 \le \phi_{k,l}^{LoS} \le \phi_{FoV}; \\ 0, & \text{Otherwise}, \end{cases} \tag{8}$$

where r is the refractive index, whose typical values are between 1 and 2 for visible light.

The channel gain of NLoS path between l^{th} LED and the k^{th} user at SC_j, which is transmitted and reflected by the n^{th} element of RIS is derived as [33]

$$h_{k,n,l}^{j} = \begin{cases} \omega_n \frac{(m+1)A_D G_f R_D}{2\pi d_{n,l}^2 d_{k,n}^2} \cos^m(\Theta_{n,l}^{NLoS}) \cos(\phi_{k,n}^{NLoS}) g(\phi_{k,n}^{NLoS}), \\ 0 \le \phi_{k,n}^{NLoS} \le \phi_{FoV}; \\ 0, \qquad \text{Otherwise.} \end{cases} \tag{9}$$

where ω_n represents the tuning coefficient of n^{th} metasurface based RIS unit. An RIS unit is conceptualized as a passive reflecting element, where the reflectivity of the element can be dynamically controlled by modifying the surface impedance using electrical voltage stimulation [21]. $d_{n,l}$ is the distance between l^{th} LED and the n^{th} element of RIS, $d_{k,n}$ is the distance between n^{th} RIS element and the k^{th} user, and $g(\phi_{k,n}^{NLoS})$.

In the considered system, transmitter sends the superimposed signal $s_j = \sum_{k=1}^{K_j} \boldsymbol{f}_{k,j} x_{k,j}$ to serve NOMA users on the j^{th} time-slot. $x_{k,j}$ is the signal intended to serve the user k on the j^{th} time-slot. All the K_j users' signals on the j^{th} time-slot should satisfy the peak amplitude constraint, that is $|x_{k,j}| \le A_p \forall k$ with mean $\mathbb{E}[x_{k,j}] = 0$ and variance $\mathbb{E}[x_{k,j}^2] = \Omega_{k,j}$ [34]. Therefore, the superimposed signal transmitted to serve NOMA users on the j^{th} time-slot is given by:

$$s_j = \sum_{k=1}^{K_j} \boldsymbol{f}_{k,j} x_{k,j} + \boldsymbol{x}_{DC}, \tag{10}$$

where $\boldsymbol{f}_{k,j} \triangleq [f_{k,j}^1, f_{k,j}^2, \ldots, f_{k,j}^L]^T \in \mathbb{R}_+^{L\times 1}$ is the precoding vector for $x_{k,j}$. $\boldsymbol{x}_{DC} \triangleq [x_{DC,1}, x_{DC,2}, \ldots, x_{DC,L}]^T \in \mathbb{R}_+^{L\times 1}$ is the direct current (DC) bias vector that ensures non-negative transmitted signal and $x_{DC,l}$ is the DC bias of the l^{th} LED [34]. To guarantee a non-negative transmitted signal, the precoding vector should satisfy:

$$\sum_{k=1}^{K_j} A_p |f_{k,j}^l| \le x_{DC,l}, \forall l \in \mathcal{L} = \{1, 2, \ldots, L\}, j \in \mathcal{J}. \tag{11}$$

Moreover, in VLC, the LEDs should satisfy the eye safety regulation as well as they have to maintain their illumination requirements. To achieve this, optical power of each LED should be limited to maximum permissible current I_p as follow

$$\sum_{k=1}^{K_j} A_p \boldsymbol{f_{k,j}}^T \boldsymbol{\aleph_l} + x_{DC,l} \le \min\{x_{DC,l}, I_p - x_{DC,l}\}, \quad \forall l \in \mathcal{L} = \{1, 2, \ldots, L\}, \quad j \in \mathcal{J}. \tag{12}$$

where, $\boldsymbol{\aleph_l}$ is a unit vector with l^{th} element equal to one. After optical-to-electrical conversion at the receivers, the received signal at k^{th} user on j^{th} time-slot is written as

$$y_{k,j} = (\boldsymbol{h}_{k,j}{}^H + \boldsymbol{\omega}_{k,j}{}^H \boldsymbol{H}_{k,j}) s_j + n_{k,j}, \tag{13}$$

Algorithm 1: User Clustering Based on Channel Gain Difference

1. **Initialization:** Total number of users K.
2. Generate channel gains: $G = [\mathbf{u}_1, \ldots, \mathbf{u}_K]$, where $\mathbf{u}_k = |\mathbf{h}_k^H + \omega_k^H \mathbf{H}_k|^2$.
3. Sort gains in descending order: $\mathbf{u}_K \geq \ldots \geq \mathbf{u}_1$.
4. Set number of clusters I.
5. Choose uniform cluster size if $K \mod I = 0$; otherwise, use varying sizes.
6. **User Grouping:**
7. Cluster 1: $\{\mathbf{u}_1, \mathbf{u}_{I+1}, \mathbf{u}_{2I+1}, \ldots, \mathbf{u}_K\}$
8. Cluster 2: $\{\mathbf{u}_2, \mathbf{u}_{I+2}, \mathbf{u}_{2I+2}, \ldots, \mathbf{u}_{K-1}\}$
9. $\vdots$
10. Cluster I: $\{\mathbf{u}_I, \mathbf{u}_{2I}, \mathbf{u}_{3I}, \ldots, \mathbf{u}_{K-I+1}\}$.

where $\boldsymbol{h}_{k,j} \triangleq [h_{k,j}^1, h_{k,j}^2, \ldots h_{k,j}^L]^T \in \mathbb{R}_+^{L\times 1}$, $\boldsymbol{\omega}_{k,j} \triangleq [\omega_{k,j}^1, \omega_{k,j}^2, \ldots, \omega_{k,j}^N]^T \in \mathbb{R}^{N\times 1}$, and $\boldsymbol{H}_{k,j} \in \mathbb{R}^{N\times L}$ which is given as

$$\boldsymbol{H}_{k,j} = \begin{bmatrix} h_{k,1,j}^1 & h_{k,1,j}^2 & \ldots & h_{k,1,j}^L \\ h_{k,2,j}^1 & h_{k,2,j}^2 & \ldots & h_{k,2,j}^L \\ \vdots & \vdots & \vdots & \vdots \\ h_{k,N,j}^1 & h_{k,N,j}^2 & \ldots & h_{k,N,j}^L \end{bmatrix}. \tag{14}$$

In Eq. (13), $n_{k,j}$ is the noise at the k^{th} user at j^{th} time-slot, which is consist of shot, thermal and relative-intensity noises. It can be modelled as additive white Gaussian noise (AWGN) with zero mean and variance $\delta_{k,j}^2$. $\delta_{k,j}^2$ can be computed as [32]

$$\delta_{k,j}^2 = 2e\alpha_{k,j}^o BW + 4\pi e A_D R_D \Upsilon BW(1 - \cos(\phi_{FoV})) + i_a^2 BW, \tag{15}$$

where e is the elementary charge, $\alpha_{k,j}^o$ is the average received optical power at the k^{th} user at j^{th} time-slot, BW denotes the system bandwidth, Υ presents the ambient light photocurrent, and i_a represent pre-amplifier noise current density.

For hybrid TDMA-NOMA enabled RIS-Assisted VLC System, user grouping and the determination of the decoding order is of great importance. The optimal grouping strategy requires an exhaustive search, which is computationally intensive. To mitigate this complexity, various sub-optimal grouping strategies have been proposed in the literature [35], [36]. In this work, we implemented user grouping based on channels gain-difference [35]. Based on the fact that SIC performs well when there is a significant difference in channel gains, we group users with the largest differences in their channel gains. After SIC, the highest channel gain user in a cluster is free from intra-cluster interference, with its throughput depending on its channel gain and power. Despite low allocated transmit power, its high channel gain ensures minimal impact on throughput. Distributing high channel gain users across different NOMA clusters enhances overall sum-throughput. Pairing low channel gain users with high channel gain users is beneficial as the latter can achieve high rates with low power, leaving more power for weaker users. The considered downlink NOMA clustering pairs the highest with the lowest channel gain user, the second highest with the second lowest, and so on. Moreover, this clustering algorithm can cluster K users with uniform cluster size if $(Kmod(I) == 0)$, otherwise with different cluster size. The detailed algorithm for the K users and I clusters case is presented in Algorithm 1.

Moreover, determining the decoding order is essential for efficient SIC implementation. Therefore, after grouping users into clusters, it is important to establish the optimal decoding order for users within each cluster. In general, the decoding order is determined by the channel gains of users [37]. It is very hard to get the optimal decoding order because of the NLoS path between the transmitter and the user, which is reflected by RIS. The reflection coefficient of RIS has a great effect on the optimal decoding order. In practice, there will be $2^{K_j T}$ different decoding orders for our proposed system, where K_j is the total number of users in each time-slot while T is the total number of time-slots in the system. For large-scale wireless systems, the exhaustive search solution for the optimal decoding order will lead to exponential growth in computational complexity. Therefore, it is important to employ low complexity decoding scheme that should base on the tunning coefficients ω_n for the determination of the sub-optimal decoding order. The formulated optimization problem for the sub-optimal decoding order determination is expressed as

$$\max_{\boldsymbol{\omega}_{k,j}} \sum_{j=1}^{J} \sum_{k=1}^{K_j} |\boldsymbol{h}_{k,j}{}^H + \boldsymbol{\omega}_{k,j}{}^H \boldsymbol{H}_{k,j}|^2, \tag{16}$$

$$s.t. \ \Big\{ 0 \leq \omega_{k,j}^n \leq 1, \quad \forall\, n \in \mathcal{N}, k \in \mathcal{K}, j \in \mathcal{J}.$$

Let,

$$\overline{\boldsymbol{H}}_{k,j} = \begin{bmatrix} \boldsymbol{H}_{k,j}\boldsymbol{H}_{k,j}{}^H & \boldsymbol{H}_{k,j}\boldsymbol{h}_{k,j} \\ \boldsymbol{h}_{k,j}{}^H \boldsymbol{H}_{k,j}{}^H & 0 \end{bmatrix}, \tag{17}$$

$$\overline{\boldsymbol{\omega}}_{k,j} = [\boldsymbol{\omega}_{k,j}, 1]^H, \tag{18}$$

$$\boldsymbol{W}_{k,j} = \overline{\boldsymbol{\omega}}_{k,j}\overline{\boldsymbol{\omega}}_{k,j}^H, \tag{19}$$

where $\boldsymbol{W}_{k,j} \succcurlyeq 0$. Then, $(\boldsymbol{h}_{k,j}{}^H + \boldsymbol{\omega}_{k,j}{}^H \boldsymbol{H}_{k,j})$ can be transformed to $\overline{\boldsymbol{\omega}}_{k,j}{}^H \overline{\boldsymbol{H}}_{k,j} \overline{\boldsymbol{\omega}}_{k,j} + |\boldsymbol{h}_{k,j}|^2$, which is equivalent to

$$Tr(\overline{\boldsymbol{H}}_{k,j}\boldsymbol{W}_{k,j}) + |\boldsymbol{h}_{k,j}|^2. \tag{20}$$

Based on these computations, the optimization problem in Eq. (16) can be written as follow

$$\max_{\boldsymbol{W}_{k,j}} \sum_{j=1}^{J} \sum_{k=1}^{K_j} Tr(\overline{\boldsymbol{H}}_{k,j}\boldsymbol{W}_{k,j}) + |\boldsymbol{h}_{k,j}|^2, \tag{21}$$

$$s.t. \ \begin{cases} 0 \leq diag(\boldsymbol{W}_{k,j}) \leq 1, \forall\, k \in \mathcal{K}, j \in \mathcal{J}, \\ \boldsymbol{W}_{k,j} \succcurlyeq 0, \forall\, k \in \mathcal{K}, j \in \mathcal{J}. \\ rank(\boldsymbol{W}_{k,j}) = 1. \end{cases}$$

The constraints in Eq. (16) are equivalently presented as in Eq. (21). The rank-one constraint in the optimization problem is non-convex. To handle this, it is transformed into a problem involving the difference of two convex functions as follows [38]

$$rank(\boldsymbol{W}_{k,j}) = 1 \Leftrightarrow tr(\boldsymbol{W}_{k,j}) - ||\boldsymbol{W}_{k,j}||_2 = 0. \tag{22}$$

The trace of matrix $\boldsymbol{W}_{k,j}$, denoted as tr($\boldsymbol{W}_{k,j}$), is the sum of its singular values, $\sum_{n=1}^{N} \lambda_n$, where λ_n represents the n^{th} largest singular value. The spectral norm of $\boldsymbol{W}_{k,j}$, denoted $||\boldsymbol{W}_{k,j}||_2$, is used in the rank-one constraint. Since this constraint is non-convex, we apply the Successive Convex Approximation (SCA) method, which approximates $||\boldsymbol{W}_{k,j}||_2$ using its first-order Taylor expansion to obtain a lower bound.

$$||\boldsymbol{W}_{k,j}||_2 \geq ||\boldsymbol{W}_{k,j}^{(t)}||_2 \,\mathrm{tr}\Big(\varkappa_{max}^{(t)} \varkappa_{max}^{(t)}{}^H (\boldsymbol{W}_{k,j} - \boldsymbol{W}_{k,j}^{(t)})\Big) \triangleq \overline{||\boldsymbol{W}_{k,j}||_2}. \tag{23}$$

In the t^{th} iteration, $\varkappa_{max}^{(t)}$ denotes the eigenvector associated with the largest singular value of matrix $\boldsymbol{W}_{k,j}$. To handle the rank-one constraint, we incorporate it into the objective

function as a penalty term, modifying the optimization problem accordingly as

$$\max_{\boldsymbol{W}_{k,j}} \sum_{j=1}^{J}\sum_{k=1}^{K_j} \mathrm{Tr}(\overline{\boldsymbol{H}}_{k,j}\boldsymbol{W}_{k,j}) + |\boldsymbol{h}_{k,j}|^2 - \eta\Big(\sum_{j=1}^{J}\sum_{k=1}^{K_j}\Big(\mathrm{tr}(\boldsymbol{W}_{k,j}) - \overline{||\boldsymbol{W}_{k,j}||_2}\Big)\Big), \quad (24)$$

$$s.t. \begin{cases} 0 \le diag(\boldsymbol{W}_{k,j}) \le 1, \forall\, k \in \mathcal{K}, j \in \mathcal{J}, \\ \boldsymbol{W}_{k,j} \succcurlyeq 0, \forall\, k \in \mathcal{K}, j \in \mathcal{J}, \end{cases}$$

where, η is the penalty factor of the rank one constraint. The optimization problem in Eq. (24) is now in standard Semidefinite programming (SDP) which can be solved through the MOSEK optimization toolbox in MATLAB. The decoding orders of NOMA users in the j^{th} subchannel can be determined by comparing their effective channel gain obtained from the solution of the optimization problem as

$$|\boldsymbol{h}_{k+1,j}{}^H + \boldsymbol{\omega}_{k+1,j}{}^H \boldsymbol{H}_{k+1,j}|^2 \ge |\boldsymbol{h}_{k,j}{}^H + \boldsymbol{\omega}_{k,j}{}^H \boldsymbol{H}_{k,j}|^2. \quad (25)$$

Based on the above decoding ordering, the received signal at k^{th} user on j^{th} time-slot after SIC can be as

$$y_{k,j} = \underbrace{(\boldsymbol{h}_{k,j}{}^H + \boldsymbol{\omega}_{k,j}{}^H \boldsymbol{H}_{k,j})\boldsymbol{f}_{k,j}x_{k,j}}_{\text{desired signal}} + \underbrace{(\boldsymbol{h}_{k,j}{}^H + \boldsymbol{\omega}_{k,j}{}^H \boldsymbol{H}_{k,j}) \sum_{m=k+1}^{K} \boldsymbol{f}_{m,j}x_{m,j}}_{\text{NOMA interference}} + n_{k,j}. \quad (26)$$

From Eq. (25), the received SINR of the k^{th} user at j^{th} time-slot after SIC is as follow

$$\gamma_{k,j} = \frac{|(\boldsymbol{h}_{k,j}{}^H + \boldsymbol{\omega}_{k,j}{}^H \boldsymbol{H}_{k,j})\boldsymbol{f}_{k,j}|^2 \Omega_{k,j}}{\sum_{m=k+1}^{K} |(\boldsymbol{h}_{k,j}{}^H + \boldsymbol{\omega}_{k,j}{}^H \boldsymbol{H}_{k,j})\boldsymbol{f}_{m,j}|^2 \Omega_{m,j} + \delta_{k,j}^2}. \quad (27)$$

In the literature, many studies specified that the achievable rate for the intensity modulation and direct detection (IM/DD) optical channel can be approximated as $BW\log_2(1+\frac{e\gamma}{2\pi})$, $BW\log_2(1+\frac{\gamma}{2\pi e})$, or $BW\log_2(1+\frac{2\gamma}{\pi e})$ with various constraints under different distributions of visible light signal [39]. As the constant coefficients with SINR γ do not affect the processing procedure of the optimization, therefore in this work the achievable rate $R_{k,j}$ of the k^{th} user at j^{th} time-slot is assumed to be computed as

$$R_{k,j} = t_j BW\log_2(1+\frac{2\gamma_{k,j}}{\pi e}). \quad (28)$$

Accordingly, the sum-rate of the each time-slot is calculated as

$$R_j = \sum_{k=1}^{K} R_{k,j}, \quad (29)$$

and the total power consumption of j^{th} time-slot is given as

$$P_j^T = \frac{1}{\xi_j}\sum_{k=1}^{K} ||\boldsymbol{f}_{k,j}||^2 + \underbrace{LP_j^d + P_j^0}_{P_j^c}, \quad (30)$$

where $\xi_j \in [0,1]$ is the power amplifier efficiency of the BS, P_j^c is the total circuit power of the transmitter, P_j^d is the dynamic power consumption, and P_j^0 is the static power consumption for the j^{th} time-slot. Now, the EE of the system can be formulated as the ratio of the sum-rate of the system to the total power consumption of the system [40], [41] as follows

$$EE_T = \frac{\sum_{j=1}^{J} R_j}{\sum_{j=1}^{J} P_j^T}. \quad (31)$$

III. Problem Formulation and its solution

The main objective is to maximize the EE of the proposed RIS-assisted downlink hybrid TDMA-NOMA VLC system. The EE of the system is maximized through the optimization of the transmit precoding and time-slot allocation for each cluster at the transmitter, and RIS tunning parameters at the RIS under required system constraints. The system constraints include illumination and optical power of LEDs, SIC decoding, data rate, power budget, time slot allocation and RIS tuning parameter. Hence, the EE optimization problem is formulated as

$$\max_{\{\boldsymbol{f}_{k,j}, t_j, \boldsymbol{\omega}_{k,j}\}} EE_T, \quad (32)$$

$$s.t. \begin{cases} C1: \sum_{k=1}^{K_j} A_p|f_{k,j}^l| \le x_{DC,l}, \quad \forall l \in \mathcal{L}, j \in \mathcal{J}, \\ C2: \sum_{k=1}^{K_j} A_p \boldsymbol{f}_{k,j}^T \boldsymbol{\aleph_l} + x_{DC,l} \le \min\{x_{DC,l}, I_p - x_{DC,l}\}, \\ \forall l \in \mathcal{L}, j \in \mathcal{J}, \\ C3: |\boldsymbol{h}_{k+1,j}{}^H + \boldsymbol{\omega}_{k+1,j}{}^H \boldsymbol{H}_{k+1,j}|^2 \ge \\ |\boldsymbol{h}_{k,j}{}^H + \boldsymbol{\omega}_{k,j}{}^H \boldsymbol{H}_{k,j}|^2, \forall j \in \mathcal{J}, k \in \mathcal{K}, \\ C4: R_{k,j} \ge R_{min}, \quad \forall j \in \mathcal{J}, k \in \mathcal{K}, \\ C5: \sum_{j=1}^{J} t_j \le t_T, \\ C6: \sum_{j=1}^{J}\sum_{k=1}^{K_j} ||\boldsymbol{f}_{k,j}||^2 \le P_{max}, \\ C7: 0 \le \omega_{k,j}^n \le 1, \quad \forall\, n \in \mathcal{N}, k \in \mathcal{K}, j \in \mathcal{J}, \end{cases}$$

where the $C1$ constraint ensures the non-negativity of the transmitted signal, $C2$ denotes the optical power constraint of each LED for the illumination requirement,$C3$ maintains SIC decoding requirements, $C4$ is to guarantee the QoS of the NOMA users in each cluster, $C5$ is the time slot allocation constraint with dynamic time, $C6$ limits the transmit power of multi-LED transmitter to P_{max}, and $C7$ is the tuning parameter constraint at each element of RIS. Constraint C3 ensures that the SIC decoding requirement is met, which relies on the reflections caused by the RIS, as explained earlier. Hence, it's crucial to use a decoding method with low complexity, which relies on tuning coefficients ω_n to decide the best decoding order. This is tackled through the optimization problem formulated in Eq. (24).

The above formulated EE maximization optimization is very challenging to solve because of the non-linear objective function and constraints. Moreover, its optimization variables are also coupled which results in its non-convexity. The problem is handled efficiently with low complexity through BCD optimization framework that solves the problem into two blocks. $A)Block1$: It handles the optimization of precoding and RIS tuning parameters. AO is applied that decouples the problem into two stages. In stage 1, for a given RIS tuning parameters and time-slot coefficients, a CQP technique is applied to optimize the transmit precoding. Then, in second stage, the RIS tuning parameters are optimized under sub-optimal precoding vectors obtained in stage 1. $B)Block2$: Then, for the optimized transmit precoding and RIS tuning parameters at block 1, the optimization problem of time-slot allocation to each cluster is solved through LP approach.

A. Block 1: Energy-Efficient transmit precoding and RIS tuning parameters optimization

First, we aim to maximize the EE of the system through optimizing transmit precoding and RIS tuning parameters through

AO framework. The optimization problem can be presented as

$$\max_{\{\boldsymbol{f}_{k,j},\boldsymbol{\omega}_{k,j}\}} EE_T, \tag{33}$$

$$s.t. \ \Big\{ C1 - C4, C6, C7.$$

The given optimization problem is non-convex because of the presence of coupled optimization variables. To address this issue, an AO framework is being utilized, which decouples the problem for each optimization variable and solves it in two stages. In the first stage, the framework optimizes $\boldsymbol{f}_{k,j}$ while holding $\boldsymbol{\omega}_{k,j}$ fixed. Once the sub-optimal $\boldsymbol{f}^*_{k,j}$ is obtained, the second stage optimizes $\boldsymbol{\omega}_{k,j}$ using the sub-optimal $\boldsymbol{f}^*_{k,j}$ obtained in the first stage. This approach decouples the optimization problem for each variable, making it easier to solve the non-convex problem efficiently.

1) Stage 1: Energy-Efficient transmit precoding: For a given RIS tunning parameters and time-slot coefficients for each cluster, the optimization problem in Eq. (32) can be simplified to a transmit precoding sub-problem given as

$$\max_{\{\boldsymbol{f}_{k,j}\}} EE_T, \tag{34}$$

$$s.t. \ \Big\{ C1, C2, C4, \& \, C6.$$

The above considered optimization problem is non-convex. Therefore, in practice, it is very difficult to get a globally optimal solution. A sequential convex programming (SCP) strategy is used to get a provably convergent iterative CQP solution. Through SCP, the problem can be transformed into the tractable form by introducing two scalar variables ψ, and Ψ total power consumption of the system and EE of the system, respectively. The equivalent transformed optimization problem can be rewritten by

$$\max_{\{\boldsymbol{f}_{k,j},\Psi,\psi\}} \Psi, \tag{35}$$

$$s.t. \ \begin{cases} C8 : EE_T \geq \Psi, \\ C9 : \sum_{j=1}^{J} R_j \geq \Psi\psi, \\ C10 : \sum_{j=1}^{J} P_j^T \leq \psi, \\ C1, C2, C4, \& \, C6. \end{cases}$$

In the above optimization problem, $C9$ and $C10$ constraints are introduced to handle the non-convex $C8$ constraint. The non-convexity of $C9$ is handled with new slack variables $\Lambda_{k,j}$ and $\zeta_{k,j}$ as

$$\begin{cases} (36a) : \log_2(1 + \frac{2\gamma_{k,j}}{\pi e}) \geq \zeta_{k,j}, & \forall k, j, \\ (36b) : 1 + \frac{2\gamma_{k,j}}{\pi e} \geq \Lambda_{k,j}, & \forall k, j, \\ (36c) : \Lambda_{k,j} \geq 2^{\zeta_{k,j}}, & \forall k, j. \end{cases} \tag{36}$$

Now, from $(36a)$, $C9$ can be equivalently written as

$$\sum_{j=1}^{J}\sum_{k=1}^{K_j} t_j BW \zeta_{k,j} \geq \Psi\psi, \forall k, j. \tag{37}$$

$C9$ in the form of Eq. (37) is still non-covex because of the coupled Ψ and ψ and its dependence on non-convex Eq. $(36b)$. To track the convexity of Eq. (37) in terms of coupled Ψ and ψ, first order Taylor expansion is exploited as

$$\sum_{j=1}^{J}\sum_{k=1}^{K_j} t_j BW \zeta_{k,j} \geq \Psi^{(i)}\psi^{(i)} + \psi^{(i)}\big(\Psi - \Psi^{(i)}\big) + \Psi^{(i)}\big(\psi - \psi^{(i)}\big), \quad \forall k, j. \tag{38}$$

where, $\Psi^{(i)}$ and $\psi^{(i)}$ indicate the value of Ψ and ψ in the i^{th} iteration. Further, to deal with the non-convexity of $(36b)$, it is relaxed by introducing variable $\mu^2_{k,j}$ as follows

$$\frac{2\Big(|(\boldsymbol{h}_{k,j}{}^H + \boldsymbol{\omega}_{k,j}{}^H \boldsymbol{H}_{k,j})\boldsymbol{f}_{k,j}|^2 \Omega_{k,j}\Big)}{\pi e\Big(\sum_{m=k+1}^{K} |(\boldsymbol{h}_{k,j}{}^H + \boldsymbol{\omega}_{k,j}{}^H \boldsymbol{H}_{k,j})\boldsymbol{f}_{m,j}|^2 \Omega_{m,j} + \delta^2_{k,j}\Big)} \geq \frac{(\Lambda_{k,j} - 1)\mu^2_{k,j}}{\mu^2_{k,j}}, \quad \forall k, j. \tag{39}$$

The above constraint can be decomposed into the following two constraints

$$(\boldsymbol{h}_{k,j}{}^H + \boldsymbol{\omega}_{k,j}{}^H \boldsymbol{H}_{k,j})\boldsymbol{f}_{k,j}\sqrt{2\Omega_{k,j}} \geq \sqrt{(\Lambda_{k,j} - 1)\mu^2_{k,j}}, \forall k, j, \tag{40}$$

and

$$\pi e\Big(\sum_{m=k+1}^{K} |(\boldsymbol{h}_{k,j}{}^H + \boldsymbol{\omega}_{k,j}{}^H \boldsymbol{H}_{k,j})\boldsymbol{f}_{m,j}|^2 \Omega_{m,j} + \delta^2_{k,j}\Big) \leq \mu^2_{k,j}, \quad \forall k, j. \tag{41}$$

The non-convexity of Eq. (40) is handled through its first order Taylor approximation of its right hand side as follows

$$(\boldsymbol{h}_{k,j}{}^H + \boldsymbol{\omega}_{k,j}{}^H \boldsymbol{H}_{k,j})\boldsymbol{f}_{k,j}\sqrt{2\Omega_{k,j}} \geq \sqrt{(\Lambda^{(i)}_{k,j} - 1)\mu^{(i)}_{k,j}{}^2} + \frac{1}{2}\sqrt{\frac{\mu^{(i)}_{k,j}{}^2}{(\Lambda^{(i)}_{k,j} - 1)}}(\Lambda_{k,j} - \Lambda^{(i)}_{k,j}) + \frac{1}{2}\sqrt{\frac{(\Lambda^{(i)}_{k,j} - 1)}{\mu^{(i)}_{k,j}{}^2}}(\mu_{k,j}{}^2 - \mu^{(i)}_{k,j}{}^2), \quad \forall k, j. \tag{42}$$

and non-convex Eq. (41) can be written in the form of convex cone constraint as presented below

$$\Bigg\| \Bigg((\boldsymbol{h}_{k,j}{}^H + \boldsymbol{\omega}_{k,j}{}^H \boldsymbol{H}_{k,j})\boldsymbol{f}_{k+1,j}\Omega_{m,j}\pi e, (\boldsymbol{h}_{k,j}{}^H + \boldsymbol{\omega}_{k,j}{}^H \boldsymbol{H}_{k,j})\boldsymbol{f}_{k+2,j}\Omega_{m,j}\pi e, \ldots, (\boldsymbol{h}_{k,j}{}^H + \boldsymbol{\omega}_{k,j}{}^H \boldsymbol{H}_{k,j})\boldsymbol{f}_{K,j}\Omega_{m,j}\pi e, \Big(\delta_{k,j}\Big)\Bigg)\Bigg\|^T_2 \leq \mu_{k,j}, \quad \forall k, j. \tag{43}$$

Furthermore, $C10$ is convex and can be written in the form of quadratic cone constraint in the following way

$$\Bigg\| \Bigg[\frac{\xi_j\psi - \xi_j P^c_j - 1}{2}, \boldsymbol{f}^T_{1,j}, \boldsymbol{f}^T_{2,j}, \ldots, \boldsymbol{f}^T_{K,j} \Bigg]^T \Bigg\|^2 \leq \frac{\xi_j\psi - \xi_j P^c_j + 1}{2}, \quad \forall j. \tag{44}$$

Moreover, constraint $C4$ can be expressed as

$$\gamma_{k,j} \geq \gamma^{min}_{k,j}, \forall k, j, \tag{45}$$

where $\gamma^{min}_{k,j} = 2^{R_{min}-1}$. The above Eq.(45) is convex and can be presented as quadratic cone constraint in the following form

$$(\boldsymbol{h}_{k,j}{}^H + \boldsymbol{\omega}_{k,j}{}^H \boldsymbol{H}_{k,j})\boldsymbol{f}_{k,j}\sqrt{2\Omega_{k,j}} \geq \gamma^{min}_{k,j} \times \Bigg\| \Big((\boldsymbol{h}_{k,j}{}^H + \boldsymbol{\omega}_{k,j}{}^H \boldsymbol{H}_{k,j})\Omega_{m,j}\pi e \Big[\boldsymbol{f}_{k+1,j}, \boldsymbol{f}_{k+2,j}, \boldsymbol{f}_{K,j}\Big], \Big(\delta_{k,j}\Big) \Bigg\|^T_2, \quad \forall k, j \tag{46}$$

Eventually, the optimization problem of transmit precoding presented in Eq. (34) can be reformulated as

$$\max \qquad \Psi, \tag{47}$$

$$s.t. \ \Big\{ C1, C2, C3, C6, (36c), (38), (42), (43), (44), \text{and } (46).$$

The above reformulated optimization problem of transmit precoding is now convex which can be solved through MATLAB CVX at the i^{th} iteration and thus it results in the desirable solution for the orignal problem in Eq.(34) in iterative manner. Initially, it is crucial to set the initial guess for the optimization variables to ensure the feasibility and convergence of the SCA-based algorithms. The sensitivity of the proposed SCA-based method necessitates carefully chosen initial values for $\{\boldsymbol{f}_{k,j}^{(0)}, t_j^{(0)}, \Psi^{(0)}, \psi^{(0)}, \Lambda_{k,j}^{(0)}, \zeta_{k,j}^{(0)}, \mu_{k,j}^{(0)}\}$. To achieve this, we identified the initial optimized precoding variables $\boldsymbol{f}_{k,j}^{(0)}$ and $t_j^{(0)}$ that maximize the sum rate of the system:

$$\max_{\boldsymbol{f}_{k,j}, t_j} \sum_{j=1}^{J} \sum_{k=1}^{K_j} R_{k,j}, \tag{48}$$

where these variables are chosen by satisfying the VLC-related constraints, such as C1 and C2, C3 regarding SIC decoding, C5 for time slot allocation, and C6 for transmit power, as presented in Eq. (32). The solution is obtained using the SCA method. As our system model includes a direct link as well as RIS, we observed that choosing random values for the RIS tuning parameters, along with feasible $\boldsymbol{f}_{k,j}^{(0)}$ and $t_j^{(0)}$, results in a feasible solution.

2) Stage 2: Energy-Efficient RIS tunning parameters: With optimized transmit precoding in stage 1, the optimization subproblem of RIS tunning parameters can be formulated as

$$\max_{\{\boldsymbol{\omega}_{k,j}\}} EE_T = \frac{\sum_{j=1}^{J} \sum_{k=1}^{K_j} R_{k,j}}{\sum_{j=1}^{J} P_j^T}, \tag{49}$$

$$s.t. \ \Big\{ C3, C4, \& \ C7.$$

The fractional objective function in Eq. (49) can be transformed to parametric form through dinkelbach algorithm as follow

$$\mathcal{F}(EE_T^{(t-1)}) = \max_{\{\boldsymbol{\omega}_{k,j}\}} \sum_{j=1}^{J} \sum_{k=1}^{K_j} R_{k,j} - EE_T^{(t-1)} \sum_{j=1}^{J} P_j^T, \tag{50}$$

Here, $EE_T^{(t-1)}$ as a real parameter represents the EE of the system computed using the values of $\boldsymbol{\omega}_{k,j}^{(t-1)}$. The notation $\boldsymbol{\omega}_{k,j}^{(t-1)}$ signifies the value of $\boldsymbol{\omega}_{k,j}$ from the previous iteration. During the first iteration, $\boldsymbol{\omega}_{k,j}^{(t-1)}$ corresponds to the initialized value of $\boldsymbol{\omega}_{k,j}$. Consequently, solving the fractional objective function presented in Eq. (49) is equal to identifying the root of the auxiliary function $\mathcal{F}(EE_T^{(t-1)})$ [42]. It can be observed that $R_{k,j}$ in Eq. (50) is not convex. Therefore, logarithmic approximation [43] is exploited to tackle its non convexity by transforming it into suitable surrogates as

$$R_{k,j} = t_j BW \Big(\chi_{k,j} \log_2(\frac{2\gamma_{k,j}}{\pi e}) + \nu_{k,j} \Big), \tag{51}$$

where

$$\chi_{k,j} = \frac{\left(\frac{2\gamma_{k,j}}{\pi e}\right)}{1 + \left(\frac{2\gamma_{k,j}}{\pi e}\right)}, \tag{52}$$

and

$$\nu_{k,j} = \log_2(1 + \frac{2\gamma_{k,j}}{\pi e}) - \chi_{k,j} \log_2(\frac{2\gamma_{k,j}}{\pi e}). \tag{53}$$

Substituting the value of $\gamma_{k,j}$ from Eq. (27) into Eq. (51) results in

$$R_{k,j} = t_j BW \Bigg[\chi_{k,j} \log_2 \left(\frac{2|(\boldsymbol{h}_{k,j}{}^H + \boldsymbol{\omega}_{k,j}{}^H \boldsymbol{H}_{k,j}) \boldsymbol{f}_{k,j}|^2 \Omega_{k,j}}{\pi e \Big(\sum_{m=k+1}^{K} |(\boldsymbol{h}_{k,j}{}^H + \boldsymbol{\omega}_{k,j}{}^H \boldsymbol{H}_{k,j}) \boldsymbol{f}_{m,j}|^2 \Omega_{m,j} + \delta_{k,j}^2 \Big)} \right) + \nu_{k,j} \Bigg]. \tag{54}$$

Let, $\tilde{f}_{k,j} = \boldsymbol{h}_{k,j}{}^H \boldsymbol{f}_{k,j}$, while $\tilde{f}_{m,j} = \boldsymbol{h}_{k,j}{}^H \boldsymbol{f}_{m,j}$. The term $\boldsymbol{F}_{k,j} = \boldsymbol{H}_{k,j} \boldsymbol{f}_{k,j}$, and $\boldsymbol{F}_{m,j} = \boldsymbol{H}_{k,j} \boldsymbol{f}_{m,j}$. Additionally, $\tilde{\boldsymbol{H}}_{k,j} = \begin{bmatrix} \boldsymbol{F}_{k,j} \boldsymbol{F}_{k,j}{}^H & \boldsymbol{F}_{k,j} \tilde{f}_{k,j}^H \\ \boldsymbol{H}_{k,j}{}^H \tilde{f}_{k,j} & 0 \end{bmatrix}$, and $\tilde{\boldsymbol{H}}_{m,j} = \begin{bmatrix} \boldsymbol{F}_{m,j} \boldsymbol{F}_{m,j}{}^H & \boldsymbol{F}_{m,j} \tilde{f}_{m,j}^H \\ \boldsymbol{F}_{m,j}{}^H \tilde{f}_{m,j} & 0 \end{bmatrix}$. Finally, $\overline{\boldsymbol{\omega}}_{k,j} = [\boldsymbol{\omega}_{k,j}, 1]^H$ and $\boldsymbol{W}_{k,j} = \overline{\boldsymbol{\omega}}_{k,j} \overline{\boldsymbol{\omega}}_{k,j}{}^H$. where $\boldsymbol{W}_{k,j} \succcurlyeq 0$. Then, $|(\boldsymbol{h}_{k,j}{}^H + \boldsymbol{\omega}_{k,j}{}^H \boldsymbol{H}_{k,j}) \boldsymbol{f}_{k,j}|^2$ and $\sum_{m=k+1}^{K} |(\boldsymbol{h}_{k,j}{}^H + \boldsymbol{\omega}_{k,j}{}^H \boldsymbol{H}_{k,j}) \boldsymbol{f}_{m,j}|^2$can be transformed to

$$Tr(\tilde{\boldsymbol{H}}_{k,j} \boldsymbol{W}_{k,j}) + |\tilde{f}_{k,j}|^2, \tag{55}$$

and

$$\sum_{m=k+1}^{K} \Big(Tr(\tilde{\boldsymbol{H}}_{m,j} \boldsymbol{W}_{k,j}) + |\tilde{f}_{m,j}|^2 \Big), \tag{56}$$

respectively. Now, Eq. (54) can be rewritten as

$$R_{k,j} = t_j BW \Bigg[\chi_{k,j} \log_2 \left(\frac{2\Big(Tr(\tilde{\boldsymbol{H}}_{k,j} \boldsymbol{W}_{k,j}) + |\tilde{f}_{k,j}|^2 \Big) \Omega_{k,j}}{\pi e \Big(\sum_{m=k+1}^{K} \Big(Tr(\tilde{\boldsymbol{H}}_{m,j} \boldsymbol{W}_{k,j}) + |\tilde{f}_{m,j}|^2 \Big) \Omega_{m,j} + \delta_{k,j}^2 \Big)} \right) + \nu_{k,j} \Bigg]. \tag{57}$$

The above equation can be expressed in more tractable form as follows

$$R_{k,j} = t_j BW \Big[\chi_{k,j} \{ \mathcal{F}_1(\boldsymbol{W}_{k,j}) - \mathcal{F}_2(\boldsymbol{W}_{k,j}) \} + \nu_{k,j} \Big], \tag{58}$$

where

$$\mathcal{F}_1(\boldsymbol{W}_{k,j}) = \log_2 \Big[2\Big(Tr(\tilde{\boldsymbol{H}}_{k,j} \boldsymbol{W}_{k,j}) + |\tilde{f}_{k,j}|^2 \Big) \Omega_{k,j} \Big], \tag{59}$$

and

$$\mathcal{F}_2(\boldsymbol{W}_{k,j}) = \log_2 \Bigg[\pi e \Bigg(\sum_{m=k+1}^{K} \Big(Tr(\tilde{\boldsymbol{H}}_{m,j} \boldsymbol{W}_{k,j}) + |\tilde{f}_{m,j}|^2 \Big) \Omega_{m,j} + \delta_{k,j}^2 \Bigg) \Bigg]. \tag{60}$$

The Eq. (58) is from the class of DC functions, therefore we resort to the surrogate optimization approach to linearly approximate $\mathcal{F}_2(\boldsymbol{W}_{k,j})$ as

$$\tilde{R}_{k,j} = t_j BW \Big[\chi_{k,j} \{ \mathcal{F}_1(\boldsymbol{W}_{k,j}) - \tilde{\mathcal{F}}_2(\boldsymbol{W}_{k,j}) \} + \nu_{k,j} \Big], \tag{61}$$

where

$$\tilde{\mathcal{F}}_2(\boldsymbol{W}_{k,j}) \triangleq \mathcal{F}_2(\boldsymbol{W}_{k,j}) \leq \mathcal{F}_2(\boldsymbol{W}_{k,j}^{(i)}) + Tr\Big(\Big[\nabla \mathcal{F}_2(\boldsymbol{W}_{k,j}^{(i)}) \Big]^H (\boldsymbol{W}_{k,j} - \boldsymbol{W}_{k,j}^{(i)}) \Big). \tag{62}$$

$\mathcal{F}_2(\boldsymbol{W}_{k,j}^{(i)})$ denotes the value of the $\mathcal{F}_2(\boldsymbol{W}_{k,j})$ in i^{th} iteration while $\nabla \mathcal{F}_2(\boldsymbol{W}_{k,j}^{(i)})$ presents the derivative of $\mathcal{F}_2(\boldsymbol{W}_{k,j})$ in i^{th} iteration. $\boldsymbol{W}_{k,j}^{(i)}$ indicates the value of $\boldsymbol{W}_{k,j}$ in i^{th} iteration.

Based on the above calculations and approximations, the optimization problem in Eq. (49) can be reformulated as

$$\max_{\{\boldsymbol{W}_j\}} \sum_{j=1}^{J}\{\sum_{k=1}^{K_j} \tilde{R}_{k,j} - EE_j P_j^T\}, \tag{63}$$

$$s.t. \begin{cases} C3: Tr(\tilde{\boldsymbol{H}}_{k+1,j}\boldsymbol{W}_{k+1,j}) + |\tilde{f}_{k+1,j}|^2 \geq \\ Tr(\tilde{\boldsymbol{H}}_{k,j}\boldsymbol{W}_{k,j}) + |\tilde{f}_{k,j}|^2, \forall j \in \mathcal{J}, k \in \mathcal{K}, \\ C4: 2\Big(Tr(\tilde{\boldsymbol{H}}_{k,j}\boldsymbol{W}_{k,j}) + |\tilde{f}_{k,j}|^2\Big)\Omega_{k,j} \geq 2^{\left\{\frac{R_{min}-\nu_{k,j}}{\chi_{k,j}}\right\}} \\ \times\Big[\pi e\Big(\sum_{m=k+1}^{K}\Big(Tr(\tilde{\boldsymbol{H}}_{m,j}\boldsymbol{W}_{k,j}) + |\tilde{f}_{m,j}|^2\Big)\Omega_{m,j} + \delta_{k,j}^2\Big)\Big], \\ \forall j \in \mathcal{J}, k \in \mathcal{K}, \\ C7: 0 \leq diag(\boldsymbol{W}_{k,j}) \leq 1, \forall\, k \in \mathcal{K}, j \in \mathcal{J}, \\ \boldsymbol{W}_{k,j} \succcurlyeq 0, \forall\, k \in \mathcal{K}, j \in \mathcal{J}. \\ rank(\boldsymbol{W}_{k,j}) = 1. \end{cases}$$

To recover the rank-one solution, the same penalty-based approach applied to the problem in Eq. (21) is utilized. This results in

$$\max_{\{\boldsymbol{W}_j\}} \sum_{j=1}^{J}\{\sum_{k=1}^{K_j} \tilde{R}_{k,j} - EE_j P_j^T\} - \eta\Big(\sum_{j=1}^{J}\sum_{k=1}^{K_j}\Big(tr(\boldsymbol{W}_{k,j}) - \overline{||\boldsymbol{W}_{k,j}||_2}\Big)\Big), \tag{64}$$

$$s.t. \begin{cases} C3, C4, C7, \\ \boldsymbol{W}_{k,j} \succcurlyeq 0, \forall\, k \in \mathcal{K}, j \in \mathcal{J}. \end{cases}$$

where, η is the penalty factor of the rank one constraint. The optimization problem in Eq. (64) is now in standard Semidefinite programming (SDP) which can be solved through the MOSEK optimization toolbox in MATLAB.

B. Block 2: Energy-Efficient time-slot allocation for each cluster

With sub-optimal $\boldsymbol{f}_{k,j}^*$, and $\boldsymbol{\omega}_{k,j}^*$ obtained in block 1, the LP- based EE maximization optimization problem of time-slot allocation for each cluster can be expressed as

$$\max_{\{\boldsymbol{t}_j\}} EE_T, \tag{65}$$

$$s.t. \begin{cases} C4, \& \, C5. \end{cases}$$

The optimization problem can be efficiently solved using standard LP solvers. We employed the Mosek optimization solver via the CVX toolbox in MATLAB. The pseudocode for the proposed BCD optimization framework for the hybrid TDMA-NOMA-based RIS-assisted downlink VLC system is presented in ***Algorithm* 2**.

C. Computational Complexity Analysis of the Proposed Algorithm:

The proposed algorithm consists of two blocks within the BCD optimization framework. **Block 1** focuses on optimizing transmit precoding and RIS tuning parameters through AO framework. Specifically, the complexity for transmit precoding optimization via CQP using MOSEK is $O(X^2Y)$, where $X = LK$ (with L as the number of LEDs and K as the total number of users) and Y is the dimension of the optimization problem. For RIS tuning parameter optimization through SDP with MOSEK, the complexity is $O(JK_jN^{3.5})$, where J is the number of time slots, K_j is the number of users in the cluster, and N is the number of RIS elements. If ω_{AO} denotes the iterations needed for the AO technique to converge, then the overall complexity of Block 1 is given by $O\left[\omega_{AO}\left(X^2Y + JK_jN^{3.5}\right)\right]$. **Block 2** employs LP to optimize the time-slot allocation for each NOMA cluster. The worst-case time complexity for solving the LP problem using MOSEK in MATLAB is $O((D+C)^{3.5})$, where D is the number of decision variables (equal to J, the number of time slots) and C is the number of constraints. If the number of iterations required for the BCD framework to converge is Ω_{BCD}, then the overall computational complexity of the proposed algorithm 2 is $\mathcal{O}\left(\Omega_{BCD}\left[\omega_{AO}\left(X^2Y + JK_jN^{3.5}\right) + (J+C)^{3.5}\right]\right)$.

Algorithm 2: Proposed BCD Optimization Framework

Initialization: noitemsep, topsep=0pt
1) Initialize system parameters.
2) Set max iterations and convergence criteria.

while *not converge* **do**
- **Block 1:**
- **AO Framework:**
- **while** *not converge* **do**
  - **Stage 1: while** *not converge* **do**
    - 1. For given t_j and $\boldsymbol{\omega}_{k,j}$, compute $\boldsymbol{f}_{k,j}$ by solving Eq. (47).
  - **end**
  - **Stage 2: while** *not converge* **do**
    - 2. With $\boldsymbol{f}_{k,j}^*$ and t_j, compute $\boldsymbol{\omega}_{k,j}$ by solving Eq. (64).
  - **end**
- **end**
- **Return** $\boldsymbol{f}_{k,j}^*$ and $\boldsymbol{\omega}_{k,j}^*$.
- **Block 2:**
- **while** *not converge* **do**
  - 3. With $\boldsymbol{f}_{k,j}^*$ and $\boldsymbol{\omega}_{k,j}^*$, compute t_j by solving Eq. (65).
- **end**
- **Return** t_j^*.

end

Return $\boldsymbol{f}_{k,j}^*$, $\boldsymbol{\omega}_{k,j}^*$, and t_j^*.

D. Convergence Analysis:

The convergence of algorithm 2 for optimizing the hybrid TDMA-NOMA-based RIS-assisted downlink VLC system is established through an iterative analysis. Let $\boldsymbol{f}_{k,j}^{(t)}$, $\boldsymbol{\omega}_{k,j}^{(t)}$, and $t_j^{(t)}$ denote the solutions at the t^{th} iteration for the respective problems in Eqs. (47), (64), and (65). The objective function, expressed as $\text{EE}(\boldsymbol{f}_{k,j}^{(t)}, \boldsymbol{\omega}_{k,j}^{(t)}, t_j^{(t)})$, demonstrates that in Block 1, the sub-optimal precoding vectors $\boldsymbol{f}_{k,j}^*$ computed for fixed $\boldsymbol{\omega}_{k,j}^{(t)}$ and $t_j^{(t)}$ yield $\text{EE}(\boldsymbol{f}_{k,j}^{(t)}, \boldsymbol{\omega}_{k,j}^{(t)}, t_j^{(t)}) \leq \text{EE}(\boldsymbol{f}_{k,j}^{(t+1)}, \boldsymbol{\omega}_{k,j}^{(t)}, t_j^{(t)})$. Similarly, in Step 5 of algorithm 2, for the given $\boldsymbol{f}_{k,j}^*$ and $t_j^{(t)}$ we get the sub-optimal RIS tunning parameter $\boldsymbol{\omega}_{k,j}^*$ by solving Eq. (64), Hence we obtain $\text{EE}(\boldsymbol{f}_{k,j}^{(t+1)}, \boldsymbol{\omega}_{k,j}^{(t)}, t_j^{(t)}) \leq \text{EE}(\boldsymbol{f}_{k,j}^{(t+1)}, \boldsymbol{\omega}_{k,j}^{(t+1)}, t_j^{(t)})$. Combining these results shows that $\text{EE}(\boldsymbol{f}_{k,j}^{(t)}, \boldsymbol{\omega}_{k,j}^{(t)}, t_j^{(t)}) \leq \text{EE}(\boldsymbol{f}_{k,j}^{(t+1)}, \boldsymbol{\omega}_{k,j}^{(t+1)}, t_j^{(t)})$, and after convergence in Block 1, we have $\text{EE}(\boldsymbol{f}_{k,j}^{(t)}, \boldsymbol{\omega}_{k,j}^{(t)}, t_j^{(t)}) \leq \text{EE}(\boldsymbol{f}_{k,j}^{*}, \boldsymbol{\omega}_{k,j}^{*}, t_j^{(t)})$. In Block 2, for the sub-optimal time allocation t_j^*, we find $\text{EE}(\boldsymbol{f}_{k,j}^{*}, \boldsymbol{\omega}_{k,j}^{*}, t_j^{(t)}) \leq \text{EE}(\boldsymbol{f}_{k,j}^{*}, \boldsymbol{\omega}_{k,j}^{*}, t_j^{(t+1)})$. This leads to the final inequality $\text{EE}(\boldsymbol{f}_{k,j}^{(t)}, \boldsymbol{\omega}_{k,j}^{(t)}, t_j^{(t)}) \leq \text{EE}(\boldsymbol{f}_{k,j}^{*}, \boldsymbol{\omega}_{k,j}^{*}, t_j^{(t+1)})$, indicating that the objective function value is nondecreasing with each iteration. Therefore, this analysis confirms that Algorithm 2 converges effectively in optimizing the hybrid TDMA-NOMA-based RIS-assisted downlink VLC system.

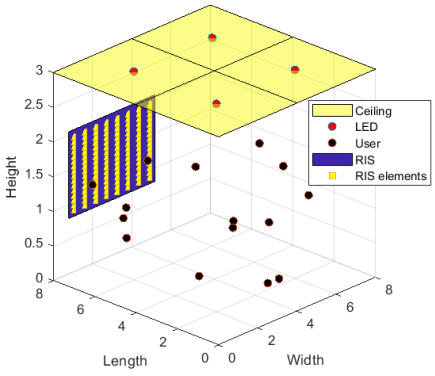

Fig. 2: SYSTEM MODEL, $L = 4$, $N = 128$, and $K = 15$.

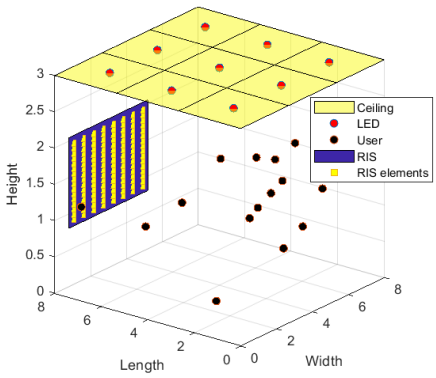

Fig. 3: SYSTEM MODEL, $L = 9$, $N = 128$, and $K = 15$.

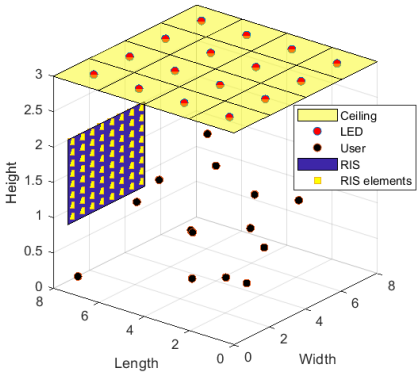

Fig. 4: SYSTEM MODEL, $L = 16$, $N = 64$, and $K = 15$.

IV. Numerical Simulations

TABLE II: Simulation Parameters

Parameter	Value
Room size	8m × 8m × 3m
Receiver FOV (ϕ_{FoV})	60°
LED emission semiangle ($\psi_{1/2}$)	70°
Area of Photodiode (A_D)	1 cm^2
Photodiode responsivity	0.45 A/W
Total transmit power	40 dBm
Refractive index (r)	1.5
Peak amplitude of signal (A_p)	2 V
Variance of input signal (Ω)	1
DC bias (x_{DC})	$\sqrt{6}\,A$
Maximum permissible current (I_p)	5 A
R_{min}	2 bits/s/Hz
Ambient light photocurrent (Υ)	10.93 A/m^2/Sr
pre-amplifier noise current density (i_a)	5 $pA/Hz^{-1/2}$

In this section, system-level simulations for optimization of transmit precoding, RIS tuning parameters and time-slot allocation for RIS-assisted TDMA-NOMA-based VLC systems are achieved through a BCD optimization framework which is analysed through the CVX toolbox in MATLAB. The performance of the proposed BCD optimization framework is evaluated using a specific simulation setup. The setup includes an 8m × 8m × 3m room with LEDs deployed on the room's ceiling. Different numbers of LEDs are analyzed during the performance analysis. For LEDs deployment, the room's ceiling is divided into perfect squares and LEDs are placed in each square's centre. The $K = 15$ single-photodiode users are deployed randomly in the room, and their locations are modeled as a BPP, unless otherwise specified. RIS consists of a rectangular frame whose two corners are (0.8m, 8m, and 0.8m), and (5m, 8m, and 2.2m). RIS units are evenly fixed in a rectangular frame, and various parameters such as Lambertian index, optical filter gain, photodiode responsivity, FOV and other simulation parameters are described in table I. The proposed algorithm is analyzed for different number of LEDS and RIS elements. The system model generated in MATLAB with different number of LEDs and RIS elements are presented in Figs 2,3, and 4.

Fig. 5 demonstrates the efficacy of the proposed algorithm in improving the EE of RIS-aided TDMA-NOMA-based VLC systems. In the simulation section, the proposed algorithm is denoted as $OTP + ORISTP + OTSC$, which achieves sub-optimal EE in three stages through a BCD optimization framework. It optimizes transmit precoding in the first stage denoted as OTP (optimized transmit precoding), RIS tuning parameters in the 2nd stage denoted as $ORISTP$ (optimized RIS tuning parameters), and time-slot coefficients of each cluster in the third stage denoted as $OTSC$ (optimized time-slot coefficients). To evaluate the effectiveness of the proposed algorithm, we compare its performance with several benchmarks. The first benchmark is random resource allocation, wherein all three optimization variables are assigned randomly. The second benchmark, denoted as OTP, optimizes only the transmit precoding while the other two optimization variables are allocated randomly. The third benchmark, denoted as $OTP{+}ORISTP$, optimizes both the transmit precoding and RIS tuning parameters while time-slot coefficients are allocated randomly. It can be observed from Fig. 5 that the proposed algorithm $(OTP{+}ORISTP{+}OTSC)$ offers the most energy-efficient solution with improvement of 13.06 % over the random resource allocation, 8.93 % over the OTP, and 4.66 % over the $OTP + ORISTP$. Moreover, it can be observed that a higher number of RIS elements results in greater EE.

Prior research on TDMA-NOMA-based VLC systems typically assumes that the available time is divided equally or deterministically among the different clusters or groups of NOMA users [44]. However, this equal or deterministic time-slot allocation can negatively impact the performance of such systems when serving groups of NOMA users with varying channel conditions. To mitigate this performance degradation, the proposed algorithm optimizes variable time slot allocation among different groups of NOMA users under their QoS constraints. Fig. 6 demonstrates the effectiveness of the proposed algorithm compared to benchmark algorithm that use fixed time-slot allocation for RIS-assisted TDMA-NOMA-based VLC systems. As shown in the figure, the proposed algorithm achieves 12.96 % higher EE than the conventional fixed time-slot allocation algorithm for $L = 16$, and 11.31 % for $L = 9$. This improvement is due to the fact that the proposed algorithm allocates more time to the clusters where NOMA users have better channel conditions, resulting in a considerable impact on the overall system performance. Thus, the proposed algorithm offers a promising solution for optimizing the time-slot allocation in RIS-assisted TDMA-NOMA-based VLC systems to achieve better performance. Moreover, it can be observed that

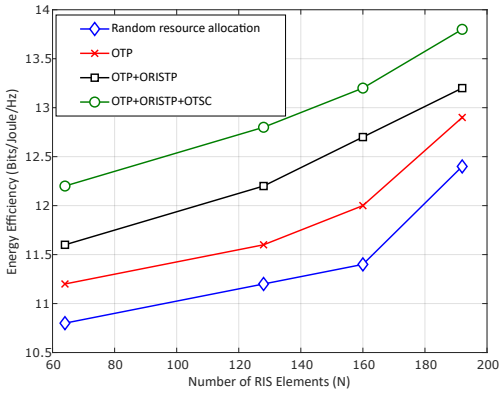

Fig. 5: Efficacy of the proposed algorithm.

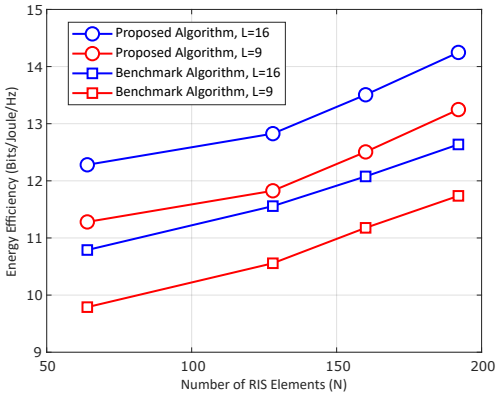

Fig. 6: EE of the proposed algorithm as compared to the benchmark.

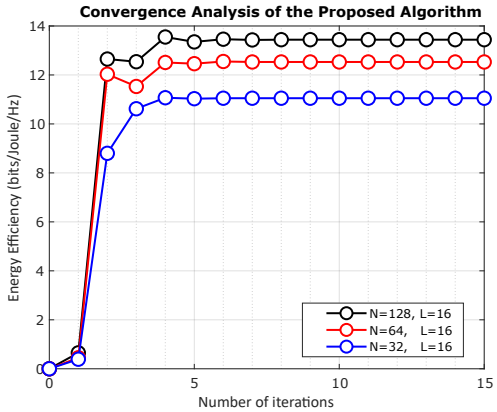

Fig. 7: Proposed algorithm convergence for various number of RIS elements.

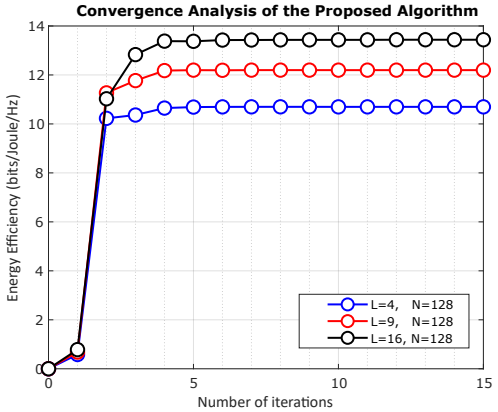

Fig. 8 : Convergence of the proposed algorithm for various number of LEDs.

by increasing the number of LEDs at the transmitter and the number of RIS elements, the system's EE can be enhanced.

Furthermore, our algorithm for solving the EE optimization problem demonstrates notable convergence towards the solution, as illustrated in Fig. 7 and Fig. 8. The results indicate that our method is effective in addressing this problem within a few iterations. Fig. 7 illustrates the convergence behavior of the proposed algorithm for different numbers of RIS elements, while Fig. 8 depicts the convergence of the algorithm for different numbers of LEDs at the transmitter. It can be observed from Figs. 7 and 8 that the proposed algorithm exhibits robustness to the number of LEDs and the number of RIS elements. This means that the proposed algorithm requires a low number of iterations to converge, regardless of various values of L and N. Furthermore, increasing the number of LEDs and RIS elements enhances the system's EE.

Fig. 9 illustrates how the system's EE is impacted by the gradual increase in circuit power, considering different number of RIS elements. The simulation results reveal that as circuit power rises, the system's EE declines. Furthermore, it can be observed from the figure that proposed algorithm can attain higher EE as compared to the conventional algorithm with fixed time-slots.

In Fig. 10 and 11, with $K = 20$ users distributed across varying numbers of clusters, it is observed that as the number of clusters increases and the number of users per cluster decreases, the overall system sum-rate improves. This enhancement in sum-rate results in better EE in the TDMA-NOMA system. Additionally, fewer users in each NOMA clusters also results in less NOMA interference. This reduction in interference allows for better utilization of the power resources among users, contributing to increase EE. Moreover, TDMA mitigates inter-cluster interference among different NOMA clusters. Therefore, Fig. 10 shows that EE increases with the number of clusters. As the number of clusters increases from 2 to 10, we compared the effectiveness of proposed algorithm for the RIS-aided TDMA-NOMA-based VLC system with a conventional algorithm as a benchmark that uses fixed time slot allocation for each cluster. Our algorithm dynamically allocates a time slot to individual clusters based on the QoS requirement of NOMA users, which results in higher EE than the benchmark. Proposed algorithm has demonstrated a significant enhancement in the EE of the system by achieving a 9 percent improvement per cluster compared to benchmark algorithm. Furthermore, it is observed that the EE increases consistently with an increase in the number of clusters. This is due to the fact that TDMA eliminates interference among clusters, and having fewer NOMA users per cluster enhances the sum-rate per cluster. As a result, a larger number of clusters in the system leads to higher EE.

Fig. 11 illustrates a comparison of the EE of the proposed algorithm with its conventional benchmark algorithm, both with and without the use of a RIS. The figure clearly demonstrates the effectiveness of the proposed algorithm in achieving an efficient solution. Additionally, the results indicate that the use of an RIS can significantly enhance the overall EE of the system by 6.5 % per cluster compared to the scenario without RIS.

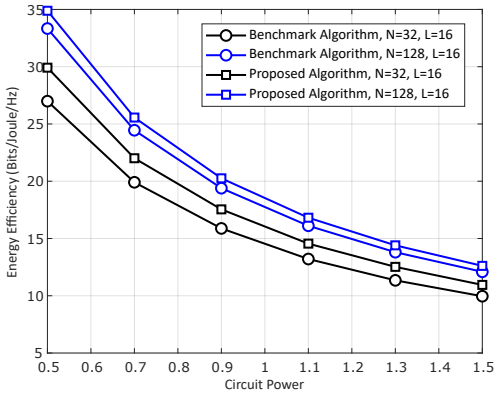

Fig. 9: EE of the system versus circuit power P_c.

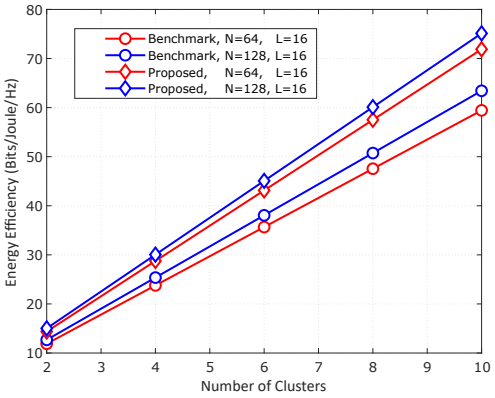

Fig. 10: EE of the system versus number of clusters.

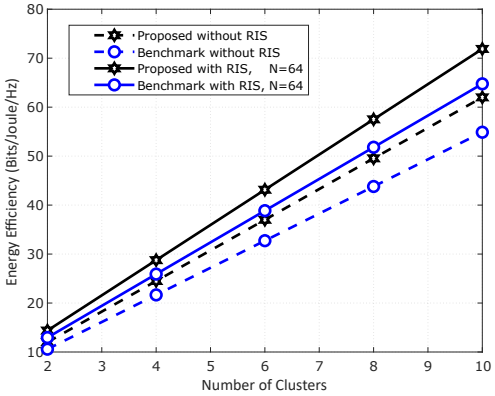

Fig. 11: EE of the system versus number of clusters (with/without RIS).

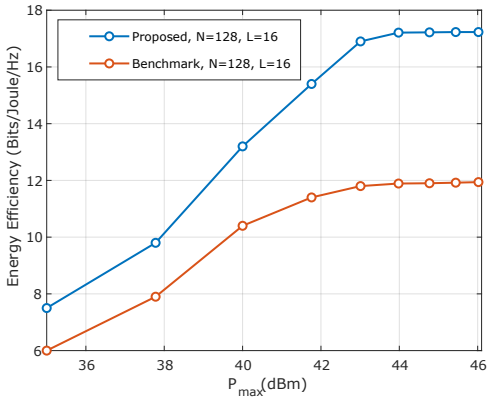

Fig. 12: EE of the system versus total transmit power budget.

Fig. 12 illustrates EE of the system as a function of total transmit power budjet (P_{max}) for proposed algorithm and it conventional benchmark with $R_{min} = 2\ bits/s/Hz$. The figure clearly highlights the superior performance of the proposed algorithm, showcasing its ability to deliver a more efficient solution as compare to its benchmark. EE initially increases with transmit power, reaching a peak before converging at higher values of P_{max} (dBm). This trend occurs because, as power rises, the system benefits from improved signal quality and data rates, which enhances EE. However, after a certain point, the additional power leads to diminishing returns due to increased energy consumption, causing the EE to stabilize. The convergence reflects the balance between improved performance and the growing cost of power, highlighting the optimal efficiency achieved by the proposed algorithm and its conventional benchmark.

V. Conclusion

In conclusion, the proposed energy-efficient optimization technique for indoor visible light communication systems using TDMA-NOMA and RIS has been successfully developed. The hybrid TDMA-NOMA approach allows for massive connectivity to multi-clusters with low computational complexity. The optimization of the precoding at the multi-LED transmitter, RIS tuning parameters, and time-slot allocation parameters for each cluster was achieved through the BCD framework, which showed excellent performance in terms of the system's EE while maintaining low computational complexity. The simulation results demonstrate the effectiveness of the proposed approach in terms of fast convergence and improved EE, which is essential for practical implementation for indoor VLC systems. Our proposed appraoch offers the energy-efficient solution with improvement of 13% for $L = 16$ over the traditional fixed time-slot allocation algorithm. This work provides a significant contribution to the field of VLC and opens up new opportunities for the development of energy-efficient indoor communication systems. For future work, the authors may explore , the user mobility and the integration of active IRS architectures [45] to further enhance system performance.

References

[1] E. Calvanese Strinati et al., "6G: The Next Frontier: From Holographic Messaging to Artificial Intelligence Using Subterahertz and Visible Light Communication," IEEE Vehicular Technology Magazine, vol. 14, no. 3, pp. 42-50, 2019.

[2] M. Z. Chowdhury, M. T. Hossan, A. Islam and Y. M. Jang, "A Comparative Survey of Optical Wireless Technologies: Architectures and Applications," IEEE Access, vol. 6, pp. 9819-9840, 2018.

[3] H. Haas, J. Elmirghani, and I. White, "Optical wireless communication," Phil. Trans. Royal Soc. A, vol. 378, no. 2169, pp. 1–11, 2020.

[4] H. Marshoud, V. M. Kapinas, G. K. Karagiannidis and S. Muhaidat, "Non-Orthogonal Multiple Access for Visible Light Communications," IEEE Photonics Technology Letters, vol. 28, no. 1, pp. 51-54, 2016.

[5] E. M. Almohimmah, M. T. Alresheedi, A. F. Abas and J. Elmirghani, "A Simple User Grouping and Pairing Scheme for Non-Orthogonal Multiple Access in VLC System," 2018 20th International Conference on Transparent Optical Networks (ICTON),pp. 1-4, 2018.

[6] Z. Ding et al., "Application of Non-Orthogonal Multiple Access in LTE and 5G Networks," IEEE Communications Magazine, vol. 55, no. 2, pp. 185-191, 2017.

[7] X. Wei, H. Al-Obiedollah, K. Cumanan, Z. Ding and O. A. Dobre, "Energy Efficiency Maximization for Hybrid TDMA-NOMA System With Opportunistic Time Assignment," IEEE Transactions on Vehicular Technology, vol. 71, no. 8, pp. 8561-8573, 2022.

[8] H. Al-Obiedollah et al., "On Energy Harvesting of Hybrid TDMA-NOMA Systems," 2019 IEEE Global Communications Conference (GLOBECOM), pp. 1-6, 2019.

[9] H. Abumarshoud, L. Mohjazi, O. A. Dobre, M. Di Renzo, M. A. Imran and H. Haas, "LiFi through Reconfigurable Intelligent Surfaces: A New Frontier for 6G?," IEEE Vehicular Technology Magazine, vol. 17, no. 1, pp. 37-46, 2022.

[10] A. M. Abdelhady, O. Amin, M. -S. Alouini and B. Shihada, "Revolutionizing Optical Wireless Communications via Smart Optics," IEEE Open Journal of the Communications Society, vol. 3, pp. 654-669, 2022.

[11] A. R. Ndjiongue, T. M. N. Ngatched, O. A. Dobre and H. Haas, "Re-Configurable Intelligent Surface-Based VLC Receivers Using Tunable Liquid-Crystals: The Concept," Journal of Lightwave Technology, vol. 39, no. 10, pp. 3193-3200, 2021.

[12] S. Aboagye, T. M. N. Ngatched, O. A. Dobre and A. R. Ndjiongue, "Intelligent Reflecting Surface-Aided Indoor Visible Light Communication Systems," IEEE Communications Letters, vol. 25, no. 12, pp. 3913-3917, 2021.

[13] M. Obeed, A. M. Salhab, M. -S. Alouini and S. A. Zummo, "On Optimizing VLC Networks for Downlink Multi-User Transmission: A Survey," IEEE Communications Surveys and Tutorials, vol. 21, no. 3, pp. 2947-2976, 2019.

[14] S. Aboagye, A. R. Ndjiongue, T. M. N. Ngatched, O. A. Dobre and H. V. Poor, "RIS-Assisted Visible Light Communication Systems: A Tutorial," IEEE Communications Surveys and Tutorials, vol. 25, no. 1, pp. 251-288, 2023.

[15] M. Asif, A. Ihsan, W. U. Khan, A. Ranjha, S. Zhang and S. X. Wu, "Energy-Efficient Backscatter-Assisted Coded Cooperative NOMA for B5G Wireless Communications," IEEE Transactions on Green Communications and Networking, vol. 7, no. 1, pp. 70-83, 2023.

[16] H. Liu, B. Huang, J. Yang, Y. Chen, T. Zhang, S. Yang and K. Chen, "Joint user grouping and power allocation in the VLC-NOMA system," Physical Communication, Volume 54, 101841, 2022.

[17] L. Yin, W. O. Popoola, X. Wu and H. Haas, "Performance Evaluation of Non-Orthogonal Multiple Access in Visible Light Communication," IEEE Transactions on Communications, vol. 64, no. 12, pp. 5162-5175, 2016.

[18] B. Cao, M. Chen, Z. Yang, M. Zhang, J. Zhao and M. Chen, "Reflecting the Light: Energy Efficient Visible Light Communication with Reconfigurable Intelligent Surface," 2020 IEEE 92nd Vehicular Technology Conference (VTC2020-Fall), Victoria, BC, Canada, pp. 1-5, 2020.

[19] S. Sun, F. Yang and J. Song, "Sum Rate Maximization for Intelligent Reflecting Surface-Aided Visible Light Communications," IEEE Communications Letters, vol. 25, no. 11, pp. 3619-3623, 2021.

[20] Z. Liu, F. Yang, S. Sun, J. Song and Z. Han, "Sum Rate Maximization for NOMA-Based VLC With Optical Intelligent Reflecting Surface," IEEE Wireless Communications Letters, vol. 12, no. 5, pp. 848-852, 2023.

[21] H. Abumarshoud, B. Selim, M. Tatipamula and H. Haas, "Intelligent Reflecting Surfaces for Enhanced NOMA-based Visible Light Communications," ICC 2022 - IEEE International Conference on Communications, Seoul, Korea, Republic of, 2022.

[22] H. Abumarshoud, C. Chen, I. Tavakkolnia, H. Haas and M. A. Imran, "Intelligent Reflecting Surfaces for Enhanced Physical Layer Security in NOMA VLC Systems," ICC 2023 - IEEE International Conference on Communications, Rome, Italy, pp. 3284-3289, 2023.

[23] H. Al-Obiedollah, H. A. B. Salameh, K. Cumanan, Z. Ding and O. A. Dobre, "Self-Sustainable Multi-IRS-Aided Wireless Powered Hybrid TDMA-NOMA System," IEEE Access, vol. 11, pp. 57428-57436, 2023.

[24] D. Zhang, Q. Wu, M. Cui, G. Zhang and D. Niyato, "Throughput Maximization for IRS-Assisted Wireless Powered Hybrid NOMA and TDMA," IEEE Wireless Communications Letters, vol. 10, no. 9, pp. 1944-1948, 2021.

[25] T. Huong Thi Le, Y. Kyaw Tun, N. Thien Thu, L. Vuong Nguyen and E. -N. Huh, "Min-Max Decoding Error Probability Optimization in RIS-Aided Hybrid TDMA-NOMA Networks," in IEEE Access, vol. 12, pp. 129720-129732, 2024.

[26] M. F. U. Abrar, M. Talha, R. I. Ansari, S. A. Hassan and H. Jung, "Optimization of STAR-RIS-Assisted Hybrid NOMA mmWave Communication," IEEE Transactions on Vehicular Technology, vol. 72, no. 8, pp. 10146-10161, 2023.

[27] J. Lei, T. Zhang and Y. Liu, "Hybrid NOMA for STAR-RIS Enhanced Communication," IEEE Transactions on Vehicular Technology, vol. 73, no. 1, pp. 1497-1502, 2024.

[28] Tiwari S, Sengupta J, Bokde ND. "Analysis of Individual User Data Rate in a TDMA-RIS-NOMA Downlink System: Beyond the Limitation of Conventional NOMA," Electronics, 12(3):618, 2023.

[29] C. Liu, L. Yu, X. Yu, J. Qian, Y. Wang and Z. Wang, "Capacity Analysis of RIS-assisted Visible Light Communication Systems with Hybrid NOMA," 2022 IEEE Globecom Workshops (GC Wkshps), Rio de Janeiro, Brazil, pp. 118-123, 2022.

[30] H. Al-Obiedollah, H. B. Salameh, K. Cumanan, Z. Ding and O. A. Dobre, "Competitive IRS Assignment for IRS-Based NOMA System," IEEE Wireless Communications Letters, vol. 13, no. 2, pp. 505-509, 2024.

[31] Q. Wu, J. Zhang and J. Guo, "Capacity Maximization for Reconfigurable Intelligent Surface-Aided MISO Visible Light Communications", Photonics, vol. 9, no. 7, p. 487, 2022.

[32] F. Xing, S. He, V. C. M. Leung and H. Yin, "Energy Efficiency Optimization for Rate-Splitting Multiple Access-Based Indoor Visible Light Communication Networks," IEEE Journal on Selected Areas in Communications, vol. 40, no. 5, pp. 1706-1720, 2022.

[33] S. Sun, F. Yang, J. Song and R. Zhang, "Intelligent Reflecting Surface for MIMO VLC: Joint Design of Surface Configuration and Transceiver Signal Processing," IEEE Transactions on Wireless Communications, vol. 22, no. 9, pp. 5785-5799, 2023.

[34] Ma, Shuai, Hui Zhou, Yijie Mao, Xiaodong Liu, Youlong Wu, Bruno Clerckx, Yuhao Wang, and Shiyin Li. "Robust beamforming design for rate splitting multiple access-aided MISO visible light communications." arXiv preprint arXiv:2108.07014, 2021.

[35] M. S. Ali, H. Tabassum and E. Hossain, "Dynamic User Clustering and Power Allocation for Uplink and Downlink Non-Orthogonal Multiple Access (NOMA) Systems," IEEE Access, vol. 4, pp. 6325-6343, 2016.

[36] W. Hao, M. Zeng, Z. Chu, and S. Yang, "Energy-efficient power allocation in millimeter wave massive MIMO with non-orthogonal multiple access," IEEE Wireless Commun. Lett., vol. 6, no. 6, pp. 782–785, 2017.

[37] L. You and D. Yuan, "A Note on Decoding Order in User Grouping and Power Optimization for Multi-Cell NOMA With Load Coupling," IEEE Transactions on Wireless Communications, vol. 20, no. 1, pp. 495-505, 2021.

[38] A. Ihsan, W. Chen, M. Asif, W. U. Khan, Q. Wu and J. Li, "Energy-Efficient IRS-Aided NOMA Beamforming for 6G Wireless Communications," IEEE Transactions on Green Communications and Networking, vol. 6, no. 4, pp. 1945-1956, 2022.

[39] A. Lapidoth, S. M. Moser and M. A. Wigger, "On the Capacity of Free-Space Optical Intensity Channels," IEEE Transactions on Information Theory, vol. 55, no. 10, pp. 4449-4461, 2009.

[40] A. Ihsan, W. Chen, S. Zhang and S. Xu, "Energy-Efficient NOMA Multicasting System for Beyond 5G Cellular V2X Communications With Imperfect CSI," IEEE Transactions on Intelligent Transportation Systems, vol. 23, no. 8, pp. 10721-10735, 2022.

[41] M. Asif, A. Ihsan, W. U. Khan, A. Ranjha, S. Zhang and S. X. Wu, "Energy-Efficient Beamforming and Resource Optimization for AmBSC-Assisted Cooperative NOMA IoT Networks," IEEE Internet of Things Journal, vol. 10, no. 14, pp. 12434-12448, 2023.

[42] A. Ihsan, W. Chen, W. U. Khan, Q. Wu and K. Wang, "Energy-Efficient Backscatter Aided Uplink NOMA Roadside Sensor Communications Under Channel Estimation Errors," IEEE Transactions on Intelligent Transportation Systems, vol. 24, no. 5, pp. 4962-4974, 2023.

[43] J. Papandriopoulos and J. S. Evans, "SCALE: A Low-Complexity Distributed Protocol for Spectrum Balancing in Multiuser DSL Networks", IEEE Transactions on Information Theory, vol. 55, no. 8, pp. 3711-3724, 2009.

[44] S. Feng, R. Zhang, W. Xu and L. Hanzo, "Multiple Access Design for Ultra-Dense VLC Networks: Orthogonal vs Non-Orthogonal," IEEE Transactions on Communications, vol. 67, no. 3, pp. 2218-2232, 2019.

[45] G. Chen, Q. Wu, C. He, W. Chen, J. Tang and S. Jin, "Active IRS Aided Multiple Access for Energy-Constrained IoT Systems," IEEE Transactions on Wireless Communications, vol. 22, no. 3, pp. 1677-1694, 2023.